euronoise

Aeroacoustic simulation based on linearized Euler equations and stochastic sound source modelling

Hervé Dechipre[a], Michael Hartmann[a], Jan Delfs[b] and Roland Ewert[b]

[a]Volkswagen AG, Brieffach 1777, 38436 Wolfsburg, Germany
[b]DLR/Institute of Aerodynamics and Flow Technology, Lilienthalplatz 7, 38108 Braunschweig, Germany
herve.dechipre@volkswagen.de

In order to continually improve passenger car acoustic comfort, effective methods are needed to simulate the noise generated by external flows as well as the noise produced by duct flows in HVAC systems. This paper presents the application of two computational aeroacoustic methods based on the Linearized Euler Equations (LEE) including 1st order non linearities and Acoustic Perturbation Equations (APE) to compute the acoustic field produced by a flat plate in a two-dimensional duct with a thickness related Reynolds number of 1300. The two methods used to investigate the noise produced are the injection of a single test-vortex in the flow and the stochastic sound source modelling by Ewert [1]. It can be shown computationally that even in the absence of the classical Aeolian tone generation resonance type phenomena occur in the duct. This paper shows the ability of both methods to simulate with accuracy resonance phenomena identified as Parker type modes [2]. The frequency and mode representation computed by both methods are in good agreement between them but also with the analytical work done by Koch [3].

1 Introduction

Improving passenger car acoustic comfort is nowadays a prime focus but require also the development of efficient numerical methods to simulate the noise produced by external flows as well as duct flows in HVAC system in the early phase of the vehicle development. Large Eddy Simulation [4] and Direct Numerical Simulation have produced good results for basic applications but hardly time and resources consuming these methods do not seem currently suitable to industrial cases.

An alternative approach consists in using steady flow simulation and an acoustic code based on Linearized Euler Equations to compute the acoustic field. To simulate the acoustic field, Lummer et al. [5] proposed to inject a vortex in the flow to generate noise by interacting with the geometry. Béchara et al. [6] introduced a stochastic model using a superposition of Fourier modes to synthesize a stochastic velocity field describing turbulence as the noise source for free turbulent flows. Recently, Ewert [1] developed a new method called Random Particle-Mesh (RPM) to set up the fluctuating turbulence velocities for broadband source noise based on the spatial filtering of white noise.

At low cruising speed, HVAC systems are generally considered as important sources of noise by car passengers. The aim of this paper is then to examine the possibility of using the test-vortex injection technique and the RPM method to compute the acoustic field generated by the flow in a duct. The geometry chosen is a 2D duct with a rounded edge thin flat plate located midway between the duct walls and at a zero angle of incidence (Fig.1). The flat plate is 0.1 m long and 2 mm thick while the duct is 0.8 m long and 0.08 m wide. The tests were carried out using the DLR's CAA code PIANO (Perturbation Investigation of Aerodynamique NOise).

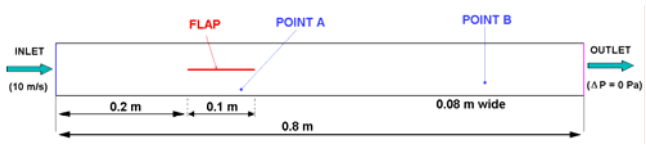

Fig.1: Duct geometry (point A is located at 80% of the chord length and point B is at 25% of the duct height)

Studying flow on parallel plates, Parker [3,7] showed the existence of resonances almost entirely caused by acoustical effects and having little or no relation to mechanical vibration of plates. Later, Koch [3] proposed analytical formulations to predict the acoustic resonance frequencies of plate cascade. Welsh et al. [8] analyzed the effect of the flow velocity on the different Parker modes in a duct containing a flat plate and pointed out that by modifying the flow velocity, the vortex shedding frequency could lock up/down to the acoustic resonant frequency.

2 Method

2.1 Calculation of the mean flow

A steady state flow field is required to initiate the acoustical calculation. The steady flow field in the duct was computed using the SST-Model developed by Menter [9] on a block structured grid composed of 158600 nodes. Three different mean flow speeds were tested: 1, 5 and 10 m/s corresponding respectively to Reynolds numbers based on the thickness of the flat plate of 128, 640 and 1300. The flow streamlines and the pressure coefficient (Cp) distribution of the steady mean flow are presented on Fig.2.

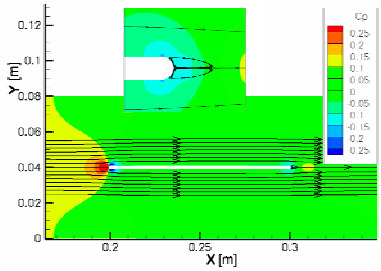

Fig.2: Steady RANS mean flow for Re = 1300; pressure coefficient Cp and streamlines

2.2 CAA Calculation

In comparison to CFD grids, CAA grids are designed with a more uniformed resolution and the grid clustering is reduced close to the walls. The steady RANS solution has to be interpolated on the acoustic grids. The effect of the grid's refinement on the acoustics results has been studied. Only minor dependencies could be identified and will not lead to further discussion in this paper. The structured grid used was composed of 12 blocks and 41900 cells.

The acoustic computation has been performed with an overall damping and no filtering. Sponge layers were placed at the inlet and outlet to avoid back waves. The spatial derivatives were approximated by the 4th order DRP-scheme [10] and the time integration is done by the

standard 4th order Runge-Kutta procedure. The numerical methods applied within PIANO are described in [11].

2.2.1 Single test-vortex injection

The interaction of vorticity with any object is a well known mechanism of sound generation and can be used to simulate the acoustic field generated by the flat plate in the duct. The method consists in injecting a single vortex in the flow which will generate noise by interacting with an obstacle. A detailed explanation of the test-vortex injection method is given by Lummer et al. [5]. Fig.3 shows the initial vortex (and the dimensionless[1] vorticity) positioned on the median line of the duct and 0.05 m forward the leading edge. Its length scale was set to $r_0 = 5\times10^{-2}$ chord length while its dimensionless strength was set 0.1 and the level of non-linearity introduced in the Euler equations was set to 10%.

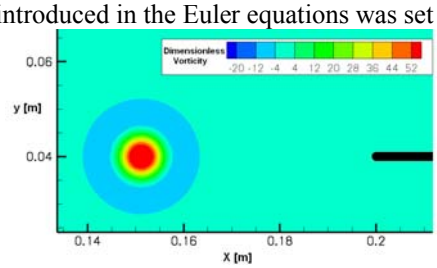

Fig.3: Initial vortex shown as dimensionless vorticity distribution

2.2.2 Random Particle Mesh (RPM)

Described in details in [1], the new stochastic RPM method is based on the spatial filtering of white noise and uses the Acoustic Perturbation Equations (APE) [12].

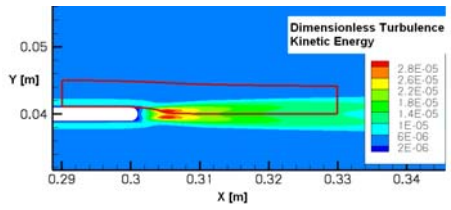

Fig. 4: Patch used for RPM (Re=1300); distribution of the dimensionless kinetic energy

A patch containing the noise sources is required to use the RPM model. Fig.4 presents the dimensionless turbulence kinetic energy and the position of the patch on which the turbulent velocity field is reconstructed. The patch is composed of 40×200 cells. Use of the symmetry was done to design the patch.

3 Results

3.1 Basic phenomena

In order to study the modes and resonances occurring in the duct, two 'virtual' pressure probes have been defined (Fig.1). The point A is positioned under the flat plate at 80% of the plate's chord and 25% of the distance between the wall and the plate. The point B is placed behind the flat plate at 3.5 times the flat plate length and at 25% of the duct height.

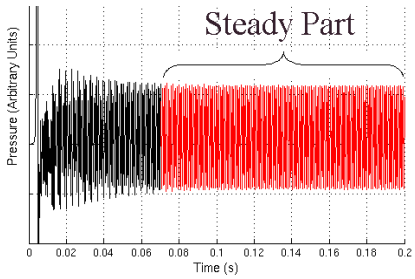

Fig.5: Temporal signal at point A (test-vortex method) Umean = 10 m/s and Plate length = 0.1 m

Fig.5 shows the temporal signal computed at both points A and B with the test-vortex injection method for a mean flow velocity of 10 m/s and a plate length of 0.1 m. The transient part in black corresponds to the interaction between the initial vortex and the geometry. In the following, only the steady phase (in red) has been used to calculate the spectrum. The spectrum was obtained by multiplying the complete pressure signal by a Hanning window and followed by a fast Fourier transform resulting in a complex spectrum for which the magnitude is shown as sound pressure level in the following.

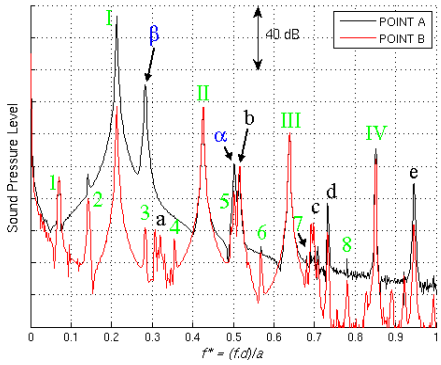

Fig.6: Spectra at points A and B (test-vortex method) U_{mean} = 10 m/s, plate length = 0.1 m

The spectra at points A and B for a vortex injection simulation have been plotted on Fig.6. The dimensionless frequency defined by Koch [3] as $f^* = (f \cdot d_0)/a_0$ was used with d_0 the height of the duct and a_0 the sound velocity. Represented on Fig.7 and identified by (I) on Fig.6 (f^* = 0.21), a vortex street due to the LEE develops behind the flat plate at a frequency of 905 Hz (corresponding to a Strouhal number based on the flat plate thickness of 0.18).

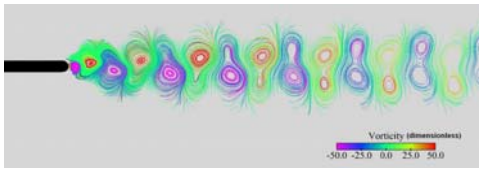

Fig.7: Vortex street St = 0.18 (Re = 1300 and L_{plate} = 0.1m)

The harmonics of this frequency are identified on Fig.6 by the capital roman numbers. Obtained by carrying out a FFT on every node of the mesh, Fig.8 gives a representation of

[1] Dimensionless quantities are calculated using the speed of sound, ambient pressure and density

the different modes or resonances. The first cut-on frequency (n=1) corresponds to f^* =0.5 for the low Mach number used. Above this frequency, propagating wave can be identified from the pictures. (II) and (III) are examples of combinations of harmonics and duct modes. The wave length for a given Mach number *(M)* of the duct mode can be calculated using Eq.1.

$$\frac{\lambda_x}{d_0} = \frac{\left(1-M^2\right)}{-f^*M + \sqrt{f^{*2} - \left(n/2\right)^2\left(1-M^2\right)}} \qquad (1)$$

The two principal β and α Parker mode [2] have also been identified for respectively dimensionless frequencies of 0.28 and 0.5. Finally, peaks designated by small numbers may be combinations of tones from the vortex street and the Parker modes while small letters corresponds to modes associated to the geometry of the duct or to combination of duct and Parker modes.

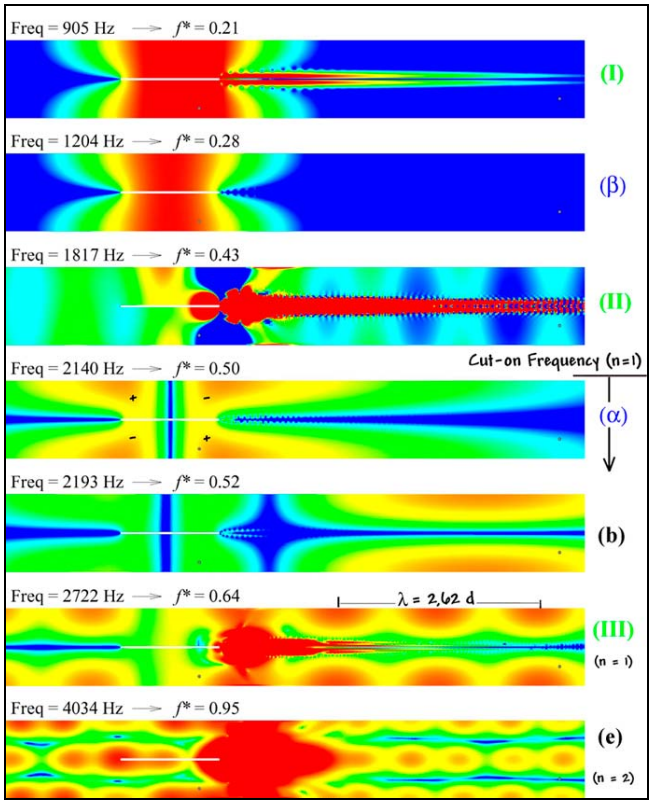

Fig.8: Map of the SPL for resonances and duct modes (U_{mean} = 10 m/s); colors of the maps are not comparable due to different scaling ranges

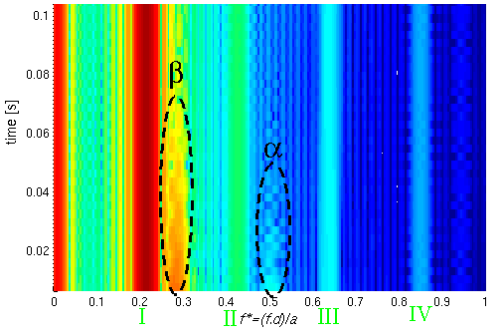

Fig.9: Spectrogram at the point A (vortex method) U_{mean} = 10 m/s, Plate length = 0.1 m

The spectrogram of the pressure signal for the point A is presented on Fig.9. In addition to the main frequencies, one can notice that as expected the intensities of α and β Parker modes (black ellipses) decrease over the time after the passage of the perturbation (vortex) due to radiation losses.

3.2 Single test-vortex injection

3.2.1 Effect of the Reynolds number

Fig.10 presents the spectra computed at point A for the same geometry and mesh resolution but at three different mean flow speeds. For a mean flow speed of 1 m/s, the acoustic level is much lower (about 100 dB) than for 10 m/s and no vortex street as well as no Parker modes has been observed. Only a duct mode is still present at f^* = 0.7. At 5 m/s the main frequency of the vortex street is visible at lower frequency but not the harmonics due to the weak non linearity, however, the level associated to the β and α Parker modes are present at the same frequencies as well as the duct modes.

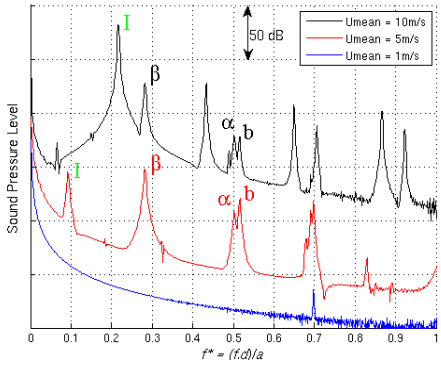

Fig.10: Spectra for 3 different mean flow velocities at point A for a plate length of 0.1 m (test-vortex method)

3.2.2 Effect of the flat plate length

For each plate length, the point A is positioned at 80% of the chord length. The spectra computed at point A for the three different plate lengths have been plotted on Fig.12. The frequency associated to the vortex street varied with the length.

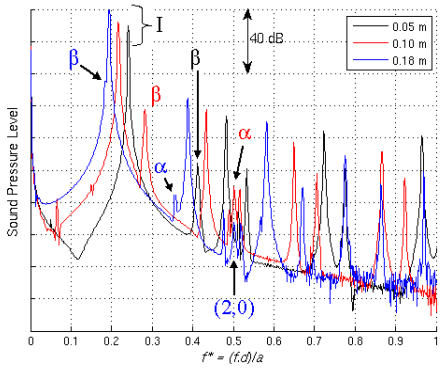

Fig.11: Spectra for 3 different plate lengths at point A for a mean flow speed of 10 m/s (test-vortex method)

Plate length	V = 10 m/s		V = 5 m/s	
	f^*	St	f^*	St
0.05 m	0.24	0.205	0.106	0.18
0.10 m	0.21	0.184	0.092	0.156
0.18 m	0.19	0.166	0.085	0.145

Table.1: Strouhal number of the vortex shedding

Table 1 gathered the frequencies and the Strouhal numbers (St) calculated using the thickness of the flat plate for each configuration. As expected [13], the smaller the plate length, the closer the Strouhal number is to the standard values of 0.2 for a cylinder.

On Fig.11, one can also see that the frequencies associated to the different Parker modes varied with the flat plate length. For the longer plate, the frequency of β Parker mode is very close to frequency of the vortex street and hardly visible of the graph. Such proximity could be an example of the lock up phenomena described by Welsh et al. [10]. A representation of different Parker modes computed for the different flat plate length is done on Fig.12. The mode (2,0) described by Koch can also be identified.

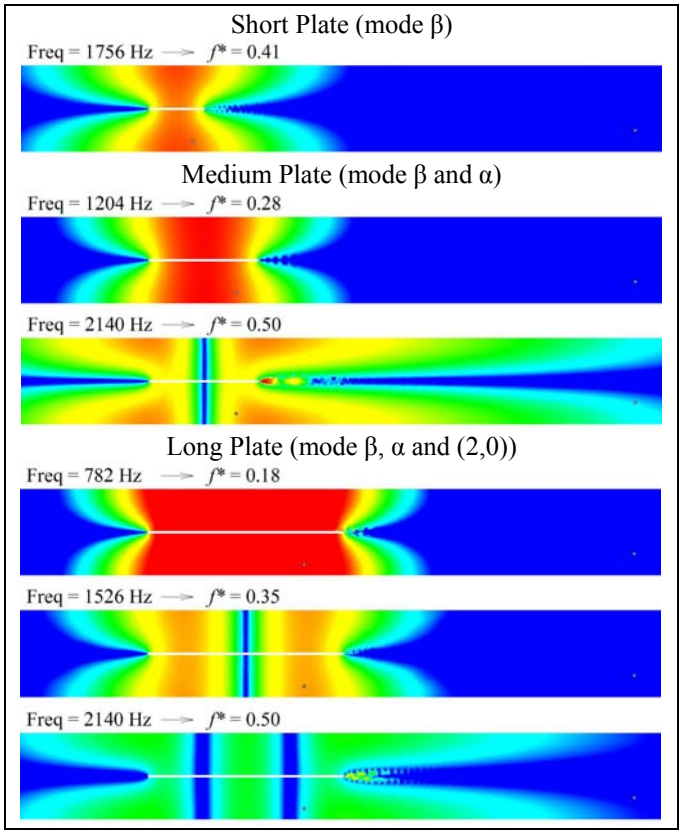

Fig.12: Maps of Parker modes simulated by test-vortex injection (U_{mean} = 10 m/s); colors of the maps are not comparable due to different scaling ranges

3.3 RPM model

3.3.1 Effect of the Reynolds number

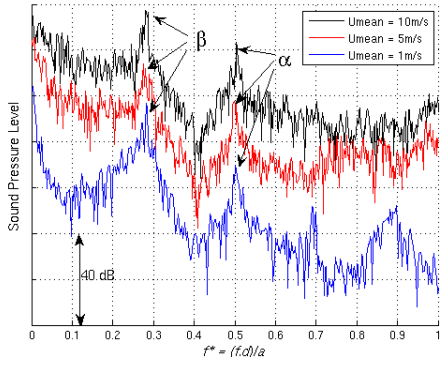

Fig.13: Spectra for 2 different mean flow velocities at point A for a plate length of 0.1 m (RPM)

Fig.13 presents the spectra obtained at point A for two different mean flow velocities. One can firstly remark, that due to the use of APE formulations, the peak corresponding to the vortex street is not present on the spectrum. Like with the previous method, the frequencies of the Parker modes do not change while their intensities decrease with the mean flow speed. At opposite to the test-vortex injection method, the Parker modes can also identified for a mean flow speed of 1 m/s. The overall lower noise level at a lower speed makes then possible to see duct modes hidden previously.

3.3.2 Effect of the flat plate length

Fig.14 presents the spectra at point A for the three different flat plate lengths computed for a mean flow speed of 10 m/s while on Fig.15 are represented the map of the Parker modes. As with the test-vortex injection, the β Parker mode is present for the three flat plate lengths. At f^* = 0.5, the modes α and (2,0) are present for respectively the plate length of 0.1 and 0.18 m.

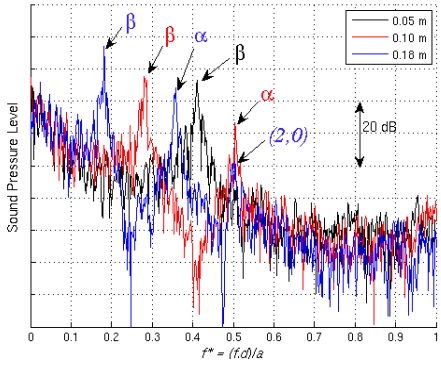

Fig.14: Spectra for 3 different plate lengths at point A for a mean flow speed of 10 m/s (RPM)

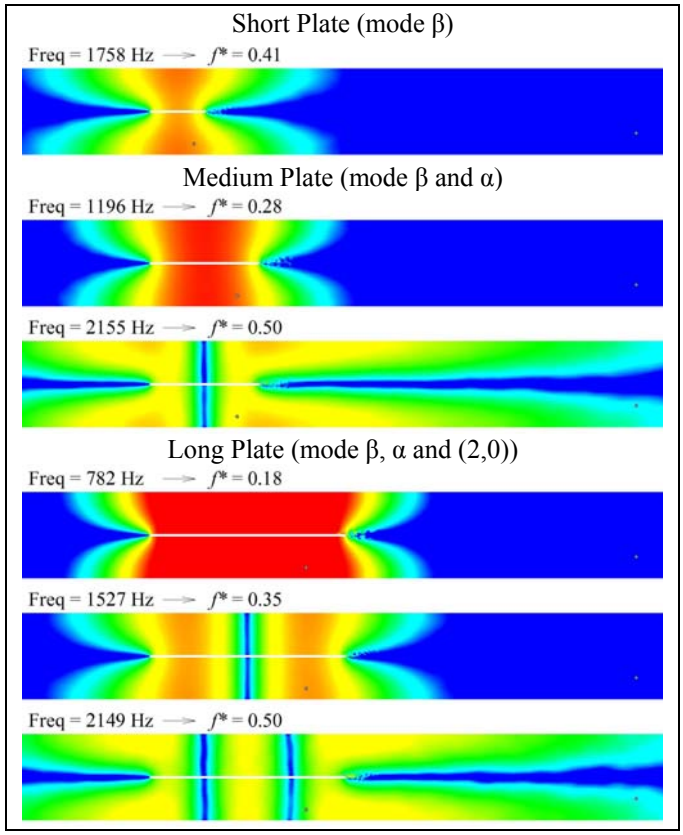

Fig.15: Maps of the Parker modes simulated by RPM (Umean = 10 m/s), colors of the maps are not comparable due to different scaling ranges

3.4 Single test-vortex injection vs. Random Particle Mesh methods

Fig.16 presents a representation of the spectra calculated at point A for the same configuration with the two different methods. It appears that the two main Parker modes are well computed with both methods. The maps of the modes represented on Fig.11 and 15 are extremely similar although the absolute level cannot be compared. The results of the test-vortex injection method are dependant on the initial intensity of the vortex making any comparison of the absolute level computed by the two methods not possible. Lastly, due to the synthesized turbulence, the RPM model produced a higher ground noise. Other duct are therefore more difficult to identify.

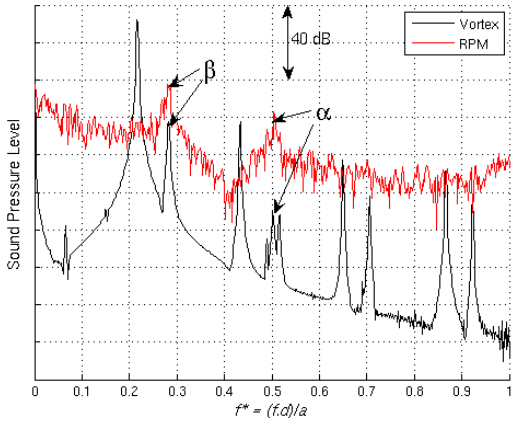

Fig.16: Comparison of the spectra obtained with the test-vortex and RPM methods at point A for a plate length of 0.1 m and a mean flow speed of 10 m/s

Fig.17 gives the evolution of the Parker against the ratio l_0/d_0 for a Mach number close to 0 after Koch [3]. The computed frequencies by the two previous methods have been also plotted on this graph.

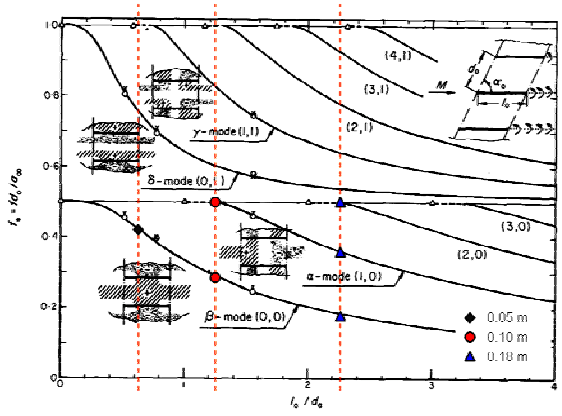

Fig.17: Evolution of the Parker Mode against the ratio l_0/d_0 after Koch [3] on which has been added the computed frequencies (marked by color points for 3 plate lengths)

The three dashed lines added on this graph correspond to the three flat plate lengths studied in this paper and the points correspond to the computed frequencies for both methods. From this graph, one can see that the results computed match well with the formulation by Koch for the low order modes. However higher duct modes could not be distinctly found by the simulations.

4 Conclusion

In this paper, two methods for aeroacoustic simulation have been tested using a simple test case of flat plate installed in a duct. Both methods have provided valuable results by predicting accurately the Parker modes for different configurations. The results of the simulations are particularly in good agreement with the calculation done by Koch.

By definition, the absolute level of the noise cannot be obtained by the vortex method; however the modes and resonances can be easily predicted. In comparison, the acoustics Parker modes can similarly be well predicted with the RPM model. By using the APE, the vortex street was suppressed but a significant ground noise is produced due to the synthesized turbulence.

References

[1] R. Ewert, Broadband slat noise prediction based on CAA and stochastic sound sources from a random particle-mesh (RPM) method, J. Comp. Fluids.

[2] R. Parker, Resonance effect in wake shedding from parallel plates: some experimental observations, J. Sound Vibr., Vol 4, 1966, pp 62-72.

[3] W. Koch, Resonant acoustic frequencies of flat plate cascades. J. Sound Vibr., Vol. 88, 1983, pp 233-242

[4] C. Wagner, T. Hüttl, P. Sagaut, Large-Eddy Simulation for Acoustics, Cambridge 2007

[5] M. Lummer, J. W. Delfs, and T. Lauke, Simulation of Sound Generation by vortices Passing the Trailing Edge of Airfoils, AIAA 2002-2578.

[6] W. Béchara, C. Bailly, P. Lafon, S. Candel, Stochastic Approach to Noise Modeling for Free Turbulent Flows, AIAA Journal, Vol. 32 - 3, 1994.

[7] R. Parker, Resonance effects in wake shedding from parallel plates: Calculation of resonant frequencies, J. Sound Vibr., Vol 5, 1967, pp 330-343

[8] M.C. Welsh, A.N. Stokes, R. Parker, Flow Resonant sound interaction in a duct containing a plate, Part I: semi-circular leading edge, JSV, 1984, 95, pp 305-323

[9] F. Menter, Zonal two equation k-w turbulence models for aerodynamic flows, AIAA Paper 93-2906

[10] C. Tam, J. Webb, Dispersion-relation-preserving finite difference schemes for computational acoustics J. Comp Phys 1993, 107, pp 262-281

[11] J. Delfs et al., Numerical Simulation of Aero-dynamic Noise with DLR´s aeroacoustic code PIANO, PIANO manual version 5.2, Brausnchweig 2007

[12] R. Ewert, W. Schröder, Acoustic Perturbation Equations based on flow decomposition via source filtering, J Comput Phys 2003, 188, p365-398

[13] E. Achenbach, Distribution of local pressure and skin friction around a circular cylinder in cross-flow up to Re=5.10^6, J. Fluid Mech., 34, pp625-639